Advanced Virgo phase cameras

XIV International Conference on Topics in Astroparticle and Underground Physics (TAUP 2015) IOP Publishing
Journal of Physics: Conference Series **718** (2016) 072008 doi:10.1088/1742-6596/718/7/072008

Advanced Virgo phase cameras

L van der Schaaf, K Agatsuma, M van Beuzekom, M Gebyehu and J van den Brand*

National Institute for Subatomic Physics, Nikhef, Amsterdam, The Netherlands
*Vrije Universiteit, Amsterdam, The Netherlands

E-mail: lschaaf@nikhef.nl

Abstract. A century after the prediction of gravitational waves, detectors have reached the sensitivity needed to proof their existence. One of them, the Virgo interferometer in Pisa, is presently being upgraded to Advanced Virgo (AdV) and will come into operation in 2016. The power stored in the interferometer arms raises from 20 to 700 kW. This increase is expected to introduce higher order modes in the beam, which could reduce the circulating power in the interferometer, limiting the sensitivity of the instrument. To suppress these higher-order modes, the core optics of Advanced Virgo is equipped with a thermal compensation system. Phase cameras, monitoring the real-time status of the beam constitute a critical component of this compensation system. These cameras measure the phases and amplitudes of the laser-light fields at the frequencies selected to control the interferometer. The measurement combines heterodyne detection with a scan of the wave front over a photodetector with pin-hole aperture. Three cameras observe the phase front of these laser sidebands. Two of them monitor the in- and output of the interferometer arms and the third one is used in the control of the aberrations introduced by the power recycling cavity. In this paper the working principle of the phase cameras is explained and some characteristic parameters are described.

1. Background and motivation

The Virgo detector is currently being upgraded in order to reach the sensitivity necessary for the detection of gravitational waves [1]. In particular, in the Advanced Virgo detector the laser power on the beam splitter of the interferometer will be increased from 0.3 to 4.9 kW. In order to suppress thermal lensing the laser power needs to be distributed evenly over the cavity mirrors. For this reason, the beam width on the input mirror will be increased from roughly two to five centimeters [1] which affects the already marginally stable power recycling cavity (PRC), as will be discussed in this section.

Figure 1-(a) shows a scheme of the optics of AdV. The laser light enters the interferometer from the left after the electro optic modulator (EOM) added sidebands to the field. These sidebands are used to control the interferometer. After the introduction of the sidebands the beam passes the input mode cleaner (IMC) to ensure a Gaussian profile. A change in length of one or both arms consisting of the input mirrors (WI and NI) and the end mirrors (WE and NE) will change the interference of the electric field at the beam splitter (BS) and is thus observable at the photodetector (DET). The two arm cavities are controlled such that the photodetector is located at the dark fringe. In order to increase the signal to noise ratio the power in the arm cavities is increased by introducing the power recycling mirror (PRM) at the light fringe, which sends the light from the light fringe back into the interferometer. The signal recycling

mirror (SRM) will be installed in about two years. Its presence alters the sensitivity curve of the instrument [1]. The output mode cleaner (OMC) makes sure only the (0,0) mode, which carries the information on the state of the interferometer arms, is detected by the photodetector.

The power recycling cavity (PRC) consists of the PRM and the two arm cavity input mirrors (WI and NI, see Figure 1-(c)). The PRC is configured such that the carrier and the indicated sidebands are resonant. However, due to the geometry of the cavity higher order modes (HOMs) can resonate for small variations in the length of the cavity, too. These HOMs interfere with the designed beam content and reduce the sensitivity of the interferometer by reducing the power of the field.

The Virgo detector already operated successfully with a marginally stable PRC. However, keeping the PRC stable for AdV is more challenging [1][2]. The Rayleigh length, z_R, increases due to the increased beam size. As a consequence the Gouy phase shift, $\phi(z) = \text{atan}\frac{z}{z_R}$ where z indicates the propagation distance from the waist of the Gaussian beam, decreases. For the effect of a smaller Gouy phase one HOM in the PRC Hermite Gaussian modes can be considered, the phase of a TEM_{mn} mode with oscillation frequency ω is given by

$$\Phi = \omega t - kz - \frac{k \cdot (x^2 + y^2)}{R(z)} + (1 + m + n) \cdot \phi(z) \tag{1}$$

where ω is the oscillation frequency of the field, k the according wave number, the field propagates in direction of z, the transverse planes have coordinates x and y, $R(z)$ is the curvature, ϕ the Gouy phase and (m, n) the mode numbers of the Hermite Gaussian mode. The expression shows that the phase depends on the mode of the electric field. Figure 1-(b) shows on the horizontal axis the acquired phase after one round trip (modulo two pi) and on the vertical axis the mean number of round trips inside the PRC for a field with according additional phase (in blue) and the mode content of the beam in the PRC (in red). The (0,0) mode is resonant in the PRC, in other words, the carrier will have the same phase after one round trip in the PRC and is indicated as red line at zero additional phase in the figure. The HOMs are indicated by the other red lines in the sketch. The HOMs lie sufficiently outside the blue resonance peak for a stable cavity. The smaller the Gouy phase the closer the HOMs lie to the carrier and the better they resonate. The increase in power (beam size) results in a smaller Gouy phase. As a consequence, the HOMs lie closer to the carrier in case of the AdV PRC than in case of the Virgo PRC.

HOMs are introduced to the electric field resonating in the PRC by surface shape errors, substrate inhomogeneities and thermal lensing. Three phase cameras are under construction: one for the PRC to detect these HOMs and two to monitor the incoming beam and the outgoing beam of the interferometer. The respective locations are indicated on the left side of Figure 1.

2. Working principle

The phase cameras in AdV measure the phase maps of the carrier and all available sidebands (up to five) at their locations simultaneously (up to 11 phase maps). In order to obtain the phase maps two beams are needed, the signal and the reference beam. The signal beam is picked up at the location of the phase camera and contains the information on the thermal status of the mirrors. The reference beam is picked up before the light enters the interferometer and is therefore not affected by aberrations of the cavities. For the interpretation of the phase maps and to reduce the noise level the phase differences between the carrier and the sideband fields are computed. In this section the working principle of the phase camera is explained and some characteristic parameters of the system are introduced.

Figure 2-(a) shows how the signal and the reference beam are recombined at the beam splitter, scanned by a scanner, and detected by a photo diode (PD). The signal beam consists of the different sidebands and the HOMs indicating the aberrations. Although the reference signal

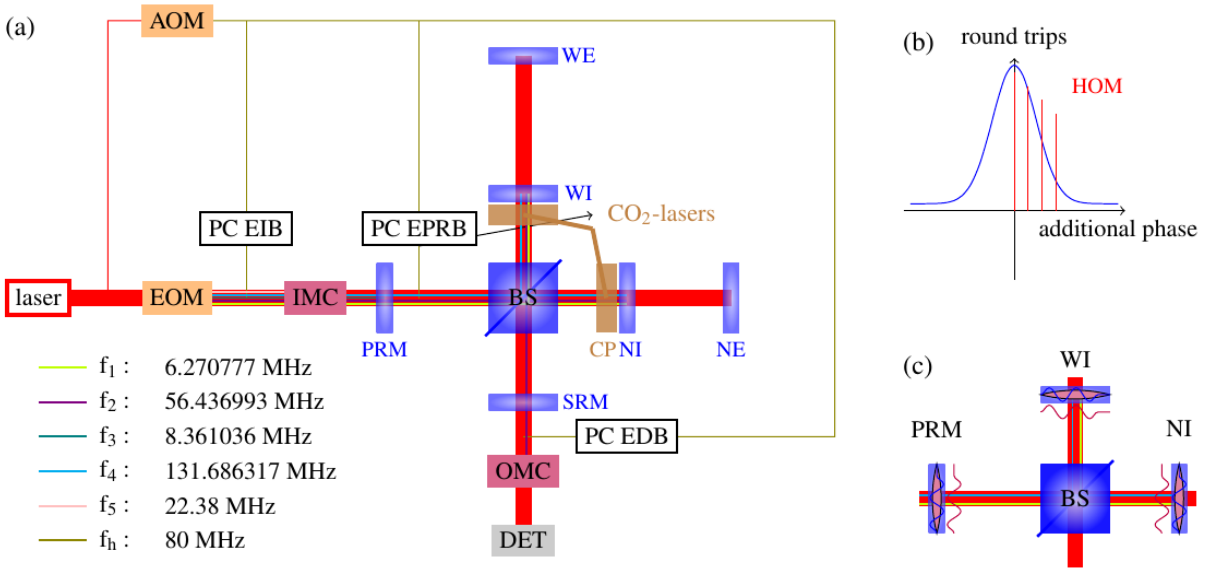

Figure 1. *(a) Sketch of AdV core optics. Three phase cameras are planned, two for monitoring purposes (PC EIB and PC EDB) and one for the TCS to suppress HOMs due to aberrations in the PRC mirrors in the PRC (PC EPRB). For acronyms consult text. (b) Vertical axis the additional Gouy phase acquired after one round trip, horizontal axis the number of round trips inside the cavity. Higher order modes can resonate for small cavity changes in a marginally stable cavity.(c) Sketch of marginally stable PRC. Higher order modes are introduced by surface shape errors, substrate inhomogeneities and thermal lensing.*

is picked up before the IMC and will contain higher order modes initially, it is passed to the respective locations with a polarization maintaining fiber which in principle filters out HOMs.

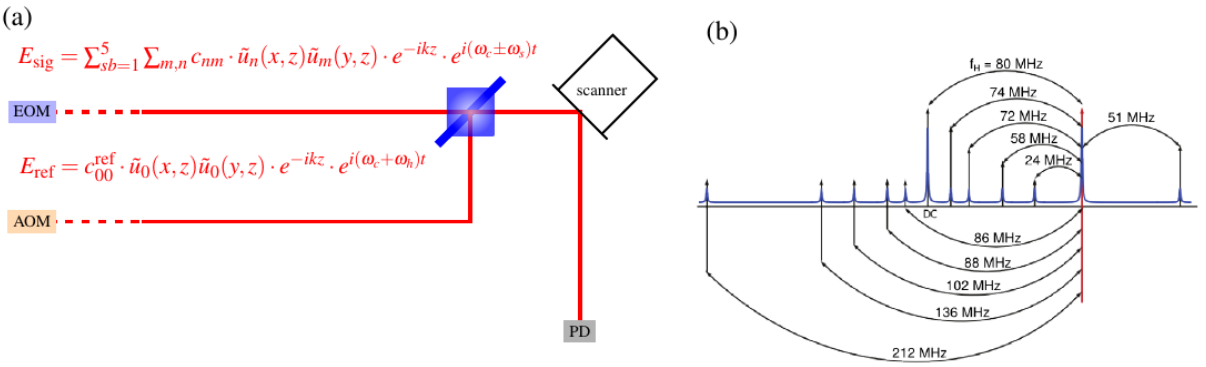

Figure 2. *(a) Layout of phase cameras. (b) The laser frequency is shifted for the heterodyne detection to resolve upper and lower sidebands. The heterodyne frequency is 80 MHz for the phase cameras. The reference frequency is indicated in red (sketch adapted from [3]).*

The electric field at the detection port is given by ($\mathcal{R}$ and $\mathcal{T}$ describe reflectivity and transitivity of the BS respectively):

$$E(\vec{x},t) = \mathcal{R} \cdot E_{\mathrm{ref}}(\vec{x},t) + i\mathcal{T} \cdot E_{\mathrm{sig}}(\vec{x},t) \tag{2}$$

The electrical current induced at a PD (in case of AdV phase camreras photodiode: OSI optoelectronics FCI-InGaAs-55 and amplifier: Hittite HMC799LP3E) is proportional to the incident beam power (proportionality factor p)[3]:

$$I(\vec{x},t) = p \cdot |E(\vec{x},t)|^2 \equiv C_1 + C_2 \cdot \sin\left[\Delta\omega t + \Delta R(\vec{x}) + \Delta\Phi(\vec{x})\right] \tag{3}$$

Where the following definitions were used:

$$\Delta R(\vec{x}) \equiv -\frac{k(x^2+y^2)}{2R_{\mathrm{ref}}} + \frac{k(x^2+y^2)}{2R_{\mathrm{sig}}} \tag{4}$$

$$\Delta\Phi(\vec{x}) \equiv k(z_{\mathrm{ref}} - z_{\mathrm{sig}}) + \phi^{\mathrm{sig}}_{\mathrm{mn}}(z_{\mathrm{sig}}) - \phi^{\mathrm{ref}}_{\mathrm{mn}}(z_{\mathrm{ref}}) \tag{5}$$

z_{ref} and z_{sig} are the distance to the reference points for the reference and the signal beam respectively, k is the wave number, x and y are the transverse coordinates, R_{sig} and R_{ref} are the curvature of signal respectively reference beam and the ϕ terms the corresponding Gouy phase shift terms. The first term, $\Delta R(\vec{x})$, contains the curvature terms and the second term, $\Delta\Phi(\vec{x})$ contains the Gouy phase shift terms of the two beams.

The photo-current oscillates with the frequency $\Delta\omega \equiv \omega_{\mathrm{ref}} - \omega_{\mathrm{sig}} = (\omega_{\mathrm{c}} + \omega_{\mathrm{h}}) - (\omega_{\mathrm{c}} \pm \omega_{\mathrm{s}}) = \omega_{\mathrm{h}} \pm \omega_{\mathrm{s}}$, with the carrier frequency ω_{c}, the heterodyne frequency ω_{h}, the sideband frequency ω_{s}. The heterodyne oscillation frequency ω_h is added by the AOM and the sideband is produced by frequency modulating the carrier, ω_{c}, with the modulation frequency ω_s of the EOM. Upper and lower sidebands are indistinguishable if the homodyne instead of the heterodyne detection principle is used, the frequency difference between reference signal and sideband would be equal for upper and lower sideband. Due to the heterodyne detection principle with as heterodyne frequency 80 MHz all frequency differences between reference signal and sidebands/carrier of the signal are mutually different (Figure 2-(b))

For the demodulation the photo-current is digitized with an analog to digital converter (ADC). The ADC used in this project samples at 500 MHz and has a resolution of 14 bit (ADC: Intersil ISLA214P50). The signal is then analyzed with a field programmable gate array (FPGA). The FPGA multiplies the digitized signal with a sine and a cosine oscillating at the frequency corresponding to the sideband of interest and low-pass filters the two quadratures:

$$I(\vec{x}) = p \cdot rt \cdot |\Psi^{\mathrm{ref}}_{\mathrm{mn}}(\vec{x})||\Psi^{\mathrm{sig}}_{\mathrm{mn}}(\vec{x})| \cdot \cos[\Delta R(\vec{x}) + \Delta\Phi(\vec{x})] \tag{6}$$

$$Q(\vec{x}) = p \cdot rt \cdot |\Psi^{\mathrm{ref}}_{\mathrm{mn}}(\vec{x})||\Psi^{\mathrm{sig}}_{\mathrm{mn}}(\vec{x})| \cdot \sin[\Delta R(\vec{x}) + \Delta\Phi(\vec{x})] \tag{7}$$

From these expressions the phase and amplitude can be determined:

$$\Delta R(\vec{x}) + \Delta\Phi(\vec{x}) = \mathrm{atan}\left[\frac{Q(\vec{x})}{I(\vec{x})}\right] \text{ and } C_2 = \sqrt{I^2(\vec{x}) + Q^2(\vec{x})} \tag{8}$$

The FPGA (Xilinx Virtex-7 XC7VX485) limits the number of samples per pixel to 2^{14} due to memory. The minimal number of samples to resolve the different sidebands is 1000 (given by the smallest frequency difference between the sidebands and the sampling frequency of the ADC of 500 MHz). For a phase map with a resolution of 128×128 pixels the scanning time is thus limited by: $0.033\ \mathrm{s} < T_{\mathrm{s}} < 0.54\ \mathrm{s}$. The upper bound is still within the specifications of 1 s [4].

3. Phase maps

The phase maps are taken with the test setup at Nikhef [5]. The maps are shown in Figure 3. The sideband in the signal beam has a frequency shift of 7 MHz with respect to the carrier. The carrier in the reference beam is shifted by the AOM by 80 MHz. The demodulation is done with 73 MHz and 80 MHz. The phase map for the sideband is pixelated at the outskirts, this is due to the low power in the beam (20 mW at PD). The innermost point of the scanning pattern

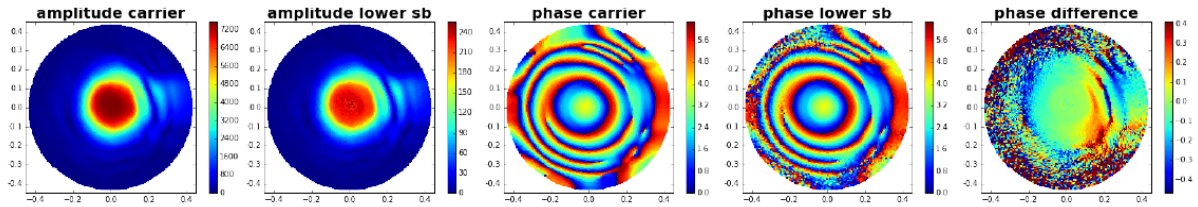

Figure 3. *Preliminary result. Data taken with the Nikhef test setup with 20 mW at the PD. This low power is responsible for the pixelated outer rim of the sideband measurement. The central value of the phase difference plot is 1.86 nm.*

for the two subtracted phase maps shows a phase difference of 1.86 nm. If the beams where perfectly aligned and in case of no noise the phase difference would be zero at the beam center. For this scan the resolution is 2^{14} pixels and the scanning time is 0.54 s. The data shows that the phase camera is able to obtain phase maps with good quality and within specifications [4].

4. Conclusions

The phase camera is a device to measure the phase front of a laser beam. In AdV three phase cameras will be used to monitor the beam and take part in the TCS. The TCS is responsible for the suppression of HOMs in the PRC. AdV without the TCS or phase cameras would not obtain the necessary sensitivity for the detection of gravitational waves. Tests of the hardware are currently ongoing and look promising. Additional to the scanning time limitations due to the frequency response of the scanner [5] (lower bound), the scanning time is limited due to the memory of the FPGA (upper bound).

Acknowledgements

The authors are grateful to Dr. David Rabeling for advice and discussion. Also, the authors thank Guido Visser and Hans Verkooijen for their technical support. This work is part of the research program of the Foundation for Fundamental Research on Matter (FOM), which is part of the Netherlands Organisation for Scientific Research (NWO).

References

[1] Virgo Collaboration 2012 *Advanced Virgo Technical Design Report. Internal note: VIR0128A12*
[2] Day R 2011 *Simulation of use of phase camera as sensor for correcting common high order aberrations in MSRC. Internal note: VIR-0389A-11*
[3] Day R, Genin E and Rocchi A 2012 *Phase camera requirements from INJ and TCS Subsystems. Internal note: VIR-0258A-12*
[4] Agatsuma K *et al* 2015 *NIM A* in press
[5] van Beuzekom M, van den Brand J and Rabeling D 2012 *ADC and DAQ Constraints for Digital Demodulation for the Advanced Virgo Phase Camera. Internal note: VIR-0304A-12*
[6] Agatsuma K *et al* 2014 *Phase camera development for gravitational wave detectors*, Proceedings of Science